Journal of Electrochemistry

Volume 30 | Issue 9

2024-09-28

Electronic Communication between Co and Ru Sites Decorated on Nitrogen-doped Carbon Nanotubes Boost the Alkaline Hydrogen Evolution Reaction

Meng-Ting Gao

Ying Wei

Xue-Meng Hu

Wenj-Jie Zhu

Qing-Qing Liu

Jin-Yuan Qiang

Wan-Wan Liu

See next page for additional authors

Recommended Citation

Meng-Ting Gao, Ying Wei, Xue-Meng Hu, Wenj-Jie Zhu, Qing-Qing Liu, Jin-Yuan Qiang, Wan-Wan Liu, Ying Wang, Xu Li, Jian-Feng Huang, Yong-Qiang Feng. Electronic Communication between Co and Ru Sites Decorated on Nitrogen-doped Carbon Nanotubes Boost the Alkaline Hydrogen Evolution Reaction[J]. *Journal of Electrochemistry*, 2024 , 30(9): 2403081.
DOI: 10.61558/2993-074X.3460
Available at: https://jelectrochem.xmu.edu.cn/journal/vol30/iss9/7

Electronic Communication between Co and Ru Sites Decorated on Nitrogen-doped Carbon Nanotubes Boost the Alkaline Hydrogen Evolution Reaction

Authors

Meng-Ting Gao, Ying Wei, Xue-Meng Hu, Wenj-Jie Zhu, Qing-Qing Liu, Jin-Yuan Qiang, Wan-Wan Liu, Ying Wang, Xu Li, Jian-Feng Huang, and Yong-Qiang Feng

Corresponding Author(s)

Yong-Qiang Feng(fengyq@sust.edu.cn)

ARTICLE

Electronic Communication Between Co and Ru Sites Decorated on Nitrogen-Doped Carbon Nanotubes Boosting the Alkaline Hydrogen Evolution Reaction

Meng-Ting Gao[#], Ying Wei[#], Xue-Meng Hu, Wenj-Jie Zhu, Qing-Qing Liu, Jin-Yuan Qiang, Wan-Wan Liu, Ying Wang, Xu Li, Jian-Feng Huang, Yong-Qiang Feng[*]

School of Materials Science and Engineering, Shaanxi University of Science and Technology, Xi'an 710021, Shaanxi, China

Abstract

Designing highly efficient Pt-free electrocatalysts with low overpotential for an alkaline hydrogen evolution reaction (HER) remains a significant challenge. Here, a novel and efficient cobalt (Co), ruthenium (Ru) bimetallic electrocatalyst composed of CoRu nanoalloy decorated on the N-doped carbon nanotubes (CoRu@N-CNTs), was prepared by reacting fullerenol with melamine via hydrothermal treatment and followed by pyrolysis. Benefiting from the electronic communication between Co and Ru sites, the as-obtained CoRu@N-CNTs catalyst exhibited superior electrocatalytic HER activity. To deliver a current density of 10 $mA \cdot cm^{-2}$, it required an overpotential of merely 19 mV along with a Tafel slope of 26.19 $mV \cdot dec^{-1}$ in 1 $mol \cdot L^{-1}$ potassium hydroxide (KOH) solution, outperforming the benchmark Pt/C catalyst. The present work would pave a new way towards the design and construction of an efficient electrocatalyst for energy storage and conversion.

Keywords: CoRu alloy; Electrocatalyst; Water splitting; Hydrogen evolution reaction; Carbon nanotubes

1. Introduction

A viable approach to addressing both the direct energy deficit and the greenhouse effect is electrocatalytic water splitting, which is a significant way to manufacture hydrogen (H_2) on a big scale and at a low cost [1—6]. In the overall water splitting process, the electrochemical hydrogen evolution reaction (HER) presents an alluring approach to producing H_2 as one of the most promising substitutes for traditional fossil fuels [7—9]. Currently, noble metal platinum (Pt) and/or Pt-based catalysts are extensively utilized as electrocatalysts for HER. Nevertheless, their exorbitant expense and restricted accessibility have impeded their widespread practical application [10—13]. Therefore, a formidable task is to find effective Pt-free electrocatalysts for HER.

Ruthenium (Ru), the most inexpensive noble metal, has emerged as the preferred substitute for Pt due to its medium-strength bond with hydrogen (about 65 $kcal \cdot mol^{-1}$) and its cost being only one-third of Pt. The inherent activity of Ru for alkaline HER is, however, greatly diminished by its restricted capacity to adsorb and dissociate H_2O [14—17]. There are two primary factors that contribute to the enhancement of catalytic activity for Ru: (1) Increasing the number of attainable active sites, which can be achieved by enlarging the specific surface area of the catalyst materials [18—22]. Generally, dispersing noble-metals on supports with high surface areas is an attractive approach to increase the number of active sites and then improve the catalytic activity [23]. (2) Improving the intrinsic activity, which is commonly accomplished by complicated structure/

Received 8 March 2024; Received in revised form 9 April 2024; Accepted 23 April 2024
Available online 23 April 2024

[#] These authors contribute equally to this work.
* Corresponding author, Yong-Qiang Feng, E-mail address: fengyq@sust.edu.cn.

https://doi.org/10.61558/2993-074X.3460

composition hybridization and electronic property tuning [13,24—26]. The chemical and electrical characteristics of Ru can be readily changed by heteroatom bond formation, improving its suitability for electrocatalytic HER [27—29]. Recently, a great deal of research has been done on diatomic catalysts (DAC), which combine to increase intrinsic activity by controlling the adsorption and desorption capacities of various metals [30—33]. The adsorption capability of the catalyst on active sites can be greatly enhanced by the action of neighboring metal atoms in DAC on the surrounding electronic environment [34,35].

Herein, a novel and efficient cobalt (Co), Ru bimetallic electrocatalyst composed of CoRu nanoalloy decorated on the N-doped carbon nanotubes (CoRu@N-CNTs), was derived from the fullerenol ($C_{60}(OH)_n$) and melamine via hydrothermal treatment followed by pyrolysis. The presence of Co catalyzed fullerenol and melamine into N-CNTs, which could serve as the electron collector. Benefiting from the strong electronic communication between Co and Ru moiety, the as-obtained CoRu@N-CNTs exhibited outperforming electrocatalytic HER activity. To deliver a current density of 10 $mA \cdot cm^{-2}$, it required an overpotential of merely 19 mV along with a Tafel slope of 26.19 $mV \cdot dec^{-1}$ in 1 $mol \cdot L^{-1}$ potassium hydroxide (KOH) solution. The present work would provide a new clue for design and construction of an efficient HER electrocatalyst.

2. Experimental section

2.1. Materials

Cobalt(II) chloride ($CoCl_2$), ethanol (EtOH, CH_3CH_2OH) and isopropyl alcohol (IPA, C_3H_8O) were purchased from Sinopharm Chemical Reagent Co., Ltd. Ruthenium (III) chloride anhydrous ($RuCl_3$), platinum on activated carbon (20 wt % Pt/C), Nafion solution (5%) and potassium hydroxide (KOH, 1.0 $mol \cdot L^{-1}$) were purchased from Sigma-Aldrich, while deionized (DI) water (resistivity: ≥18.25 MΩ·cm) was provided by an ultrapure water system (ULUPURE, UPDR-I-10 T). All the chemicals are of analytical grade and were used directly without further treatment.

2.2. Synthesis of CoRu@N-CNTs

The preparation procedure of CoRu@N-CNTs is schematically illustrated in Scheme 1. Briefly, 1.2 g of melamine, 150 mg of $C_{60}(OH)_n$, 0.5 mmol of $CoCl_2$ and 0.5 mmol of $RuCl_3$ were dissolved into 70 mL of deionized water. The mixture solution was then transferred to a stainless-steel capped Teflon autoclave. After hydrothermal treatment at 150 °C for 24 h, the solid precursor of CoRu@N-CNTs was obtained by extraction filtration. Then the obtained powder was carbonized in a tube furnace under Ar/H_2 (5%) flow for 3 h at 600 °C with a raising rate of 5 $°C \cdot min^{-1}$. After cooling naturally to the room temperature, the CoRu@N-CNTs was successfully prepared. For comparison, CoRu@NC, Co@N-CNTs and Ru@NC were also prepared following a similar procedure to CoRu@N-CNTs except in the absences of $C_{60}(OH)_n$, $RuCl_3$ and $CoCl_2$, respectively. For detail, please see in the Supporting Information.

2.3. Material characterization

X-ray diffraction (XRD) spectra were recorded on a Rigaku D/max-2200PC diffractometer (Japan) using Cu *Kα* radiation. Raman spectroscopic measurements were conducted on a Renishaw-

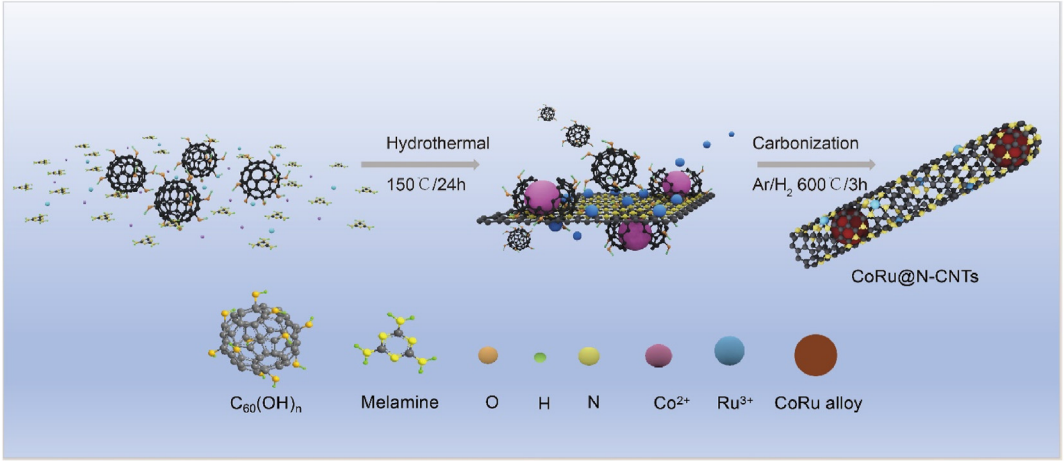

Scheme 1. Schematic illustration for the synthesis process of CoRu@N-CNTs.

invia microscopic confocal laser Raman spectrometer with 532 nm as the excitation laser. The morphology was tested using a field-emission scanning electron microscope (SEM, Hitachi S-4800). The microstructure and elemental mapping analysis were investigated by transmission electron microscope (TEM) exerted on a FEI Tecnai G2 F20 S-TWIN instrument. X-ray photoelectron spectroscopic (XPS) data were recorded on the Thermo Scientific ESCA Lab 250Xi with 200 W monochromated Al $K\alpha$ radiation.

2.4. Electrochemical measurement

The HER test was performed on the electrochemical workstation (CHI 660E, Chenhua, Shanghai) using a three-electrode system in Ar-saturated 1 mol·L^{-1} KOH. The glassy carbon electrode (GCE), graphite rod and Hg/HgO were selected as the working, counter and reference electrodes, respectively. All the potentials collected in this work were calibrated against reversible hydrogen electrode (RHE), using Pt foil as the working electrode and Pt wire as the counter electrode [36]. Therefore, the potentials with respect to RHE can be converted by the equation of E (V vs. RHE) = E (Hg/HgO) + 0.932. The electrochemical impedance spectroscopic (EIS) measurement was performed within the frequency range from 100 kHz to 0.1 Hz at a potential corresponding to the current density of 10 mA·cm^{-2} [37]. The cyclic voltammogram (CV) curves were tested in 1 mol·L^{-1} KOH in the non-Faradic region with scanning rates of 2, 4, 6, 8, 10 and 12 mV·s^{-1}. Double layer capacity (C_{dl}) could be obtained by plotting the current difference of the CV curves. Therefore, the electrochemical active surface area (ECSA) can be determined by the equation of ECSA = C_{dl}/(C_S × S), where C_S is the specific capacitance (herein 0.04 mF·cm^{-2}), and S is the surface geometric area of the electrode [38].

3. Results and discussion

3.1. Structural characterization of CoRu@N-CNTs

The synthesis route of CoRu@N-CNTs is schematically illustrated in Scheme 1. During the hydrothermal process, the as-formed CoRu nanoparticles were grafted on the surface of fullerenol, which was subsequently cracked into pieces of bowl-like carbon fragments and emerged to N-doped CNTs in the presence of melamine in the following annealing step [39]. From the SEM and TEM images shown in Fig. 1a and b, it can be found a plenty of CNTs decorated with metal

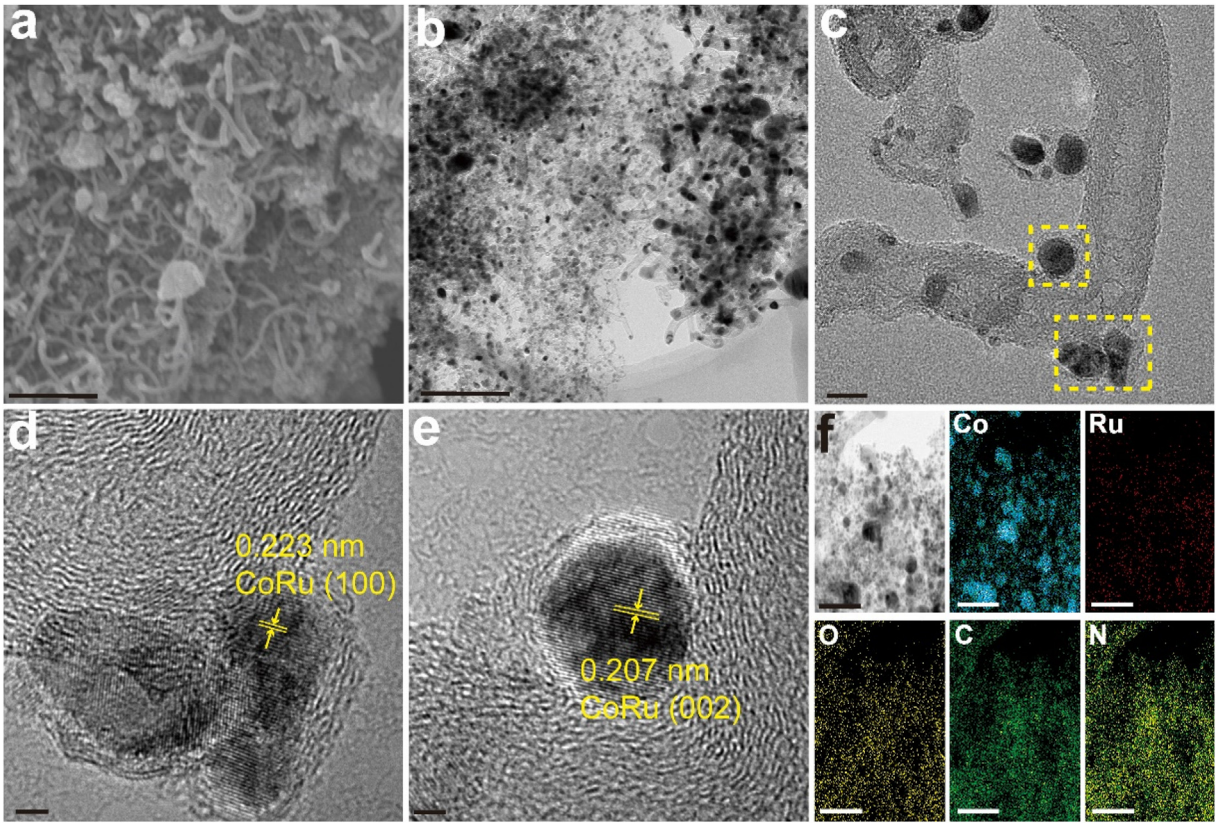

Fig. 1. Structure characterization of CoRu@N-CNTs. (a) SEM, (b) TEM, (c), (d) and (e) HRTEM images and (f) the corresponding elemental mapping images of Co, Ru, O, C and N for CoRu@N-CNTs. Scale bars in (a) 1 μm, (b) 200 nm, (c) 10 nm, (d) 2 nm, (e) 2 nm and (f) 100 nm.

nanoparticles. To further clarify the microstructure of CoRu@N-CNTs, high-resolution TEM (HRTEM) images were collected as displayed in Fig. 1c. Clearly, the CoRu nanoparticles were distributed both on the surface and inner wall of CNTs. The crystal lattice fringe of 0.223 nm (Fig. 1d) and 0.207 nm (Fig. 1e) could be assigned to the (100) and (111) facets of CoRu alloy, respectively [40]. While in the absence of $C_{60}(OH)_n$, the CoRu nanoparticles were embedded on the planar N-doped carbon matrix in CoRu@NC (Fig. S1). As for Co@N-CNTs, the Co nanoparticles were mainly enwrapped inside the CNTs (Fig. S2). Whereas in the absence of Co precursor, $C_{60}(OH)_n$ and melamine were difficult to be transformed to CNTs [23], resulting in a N-dopped carbon substrate decorated with Ru nanoparticles in Ru@NC (Fig. S3). Therefore, it was Co that catalytically promote the $C_{60}(OH)_n$ together with melamine to generate N-doped CNTs in CoRu@N-CNTs. In this case, Co nanoparticles were in a large proportion encapsulated inside the CNTs while Ru was decorated on the surface of CNTs, as demonstrated by the energy dispersive X-ray spectroscopic (EDS) mapping of CoRu@N-CNTs (Fig. 1f). As a result, CNTs served as the electron collector that accelerated the charge communication between the inner Co and outer Ru to boost the HER activity.

The crystal phase structure of CoRu@N-CNTs was then investigated by XRD. As can be seen from Fig. 2a, the diffraction peaks at 44.2°, 51.5° and 75.8° for the Co@N-CNTs can be well indexed to the (111), (200) and (220) facets of Co with a face-centered cubic crystal structure (PDF #15-0806) [40], respectively. And the peaks at 38.4°, 42.2° and 44.0° in the Ru@NC were attributed to the (100), (002) and (101) crystal lattices of hexagonal Ru (PDF#06-0663) [36], respectively. Fascinatingly, only a broadened peak around 44.0° assigned to the CoRu alloy (PDF#65-8975) with a slight upshift relative to Co@N-CNTs and Ru@NC was observed for the CoRu@N-CNTs, probably owing to the strong electronic communication between Co and Ru within the catalyst. Similar situation was also observed with the CoRu@NC. Besides, the broad signal around 26° could be assigned to the graphitic carbon. Raman spectroscopy was also used to further explore the microstructure of CoRu@N-CNTs. As displayed in Fig. 2b, the D band (1345 cm^{-1}) and G band (1586 cm^{-1}) can be observed apparently [41], indicating the coexistence of disordered and graphitic carbon in the substrate. The values of integrated intensity ratio (I_D/I_G) were determined to be 1.08, 0.85, 0.98, 0.87 for the CoRu@N-CNTs, CoRu@NC, Co@N-CNTs and Ru@NC, respectively, which is indicative of a higher degree of defects in the CoRu@N-CNTs.

XPS was employed to examine the chemical states and surface element distribution of the samples. In line with the EDS results, the survey spectra demonstrated the existences of C, N, O, Co, and Ru elements in the CoRu@N-CNTs (Fig. S4 and Table S1). The lack of Cl element excluded the contribution to electrochemical process (Fig. S5). The high-resolution XPS spectra of Co 2p is displayed in Fig. 3a. Two peaks, corresponding to Co 2p3/2 and Co 2p1/2 of metallic Co (Co^0), respectively, at 778.67 eV and 793.79 eV were observed in the CoRu@N-CNTs. While the Co^{2+} is responsible for the peaks at 781.21 eV (Co 2p3/2) and 796.73 eV (Co 2p1/2), and the set of peaks at 802.6 eV and 785.55 eV are satellite peaks [42,43]. Fig. 3b displayed the high-resolution spectrum of Ru 3p. Two distinct peak groups were visible for the CoRu@N-CNTs. The peaks located at 461.87 eV and 484.27 eV could be assigned to the 3p3/2 and 3p1/2 of Ru, corresponding to metallic Ru (Ru^0). While another set of peaks at 464.81 eV and 487.21 eV were responsible for oxidized Ru species [44,45]. It is worth noting that

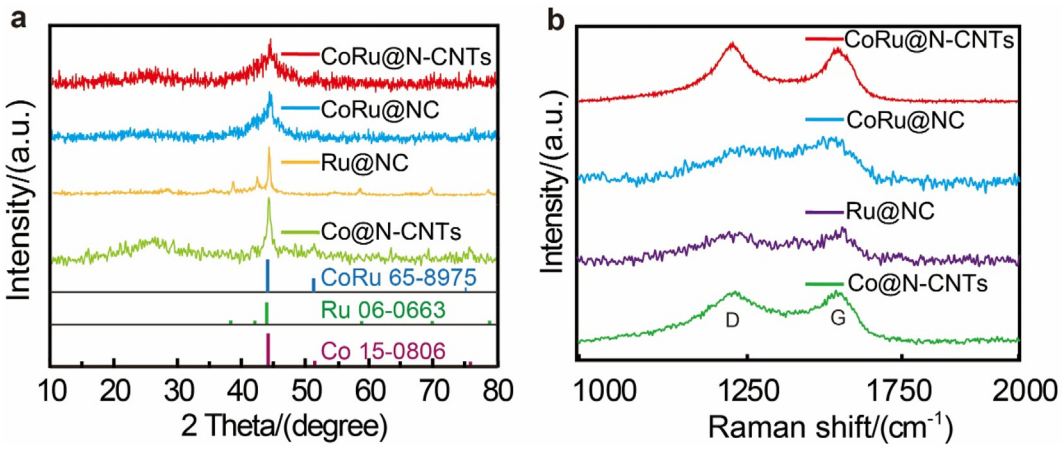

Fig. 2. (a) XRD patterns and (b) Raman spectra of the CoRu@N-CNTs, CoRu@NC, Ru@NC and Co@N-CNTs.

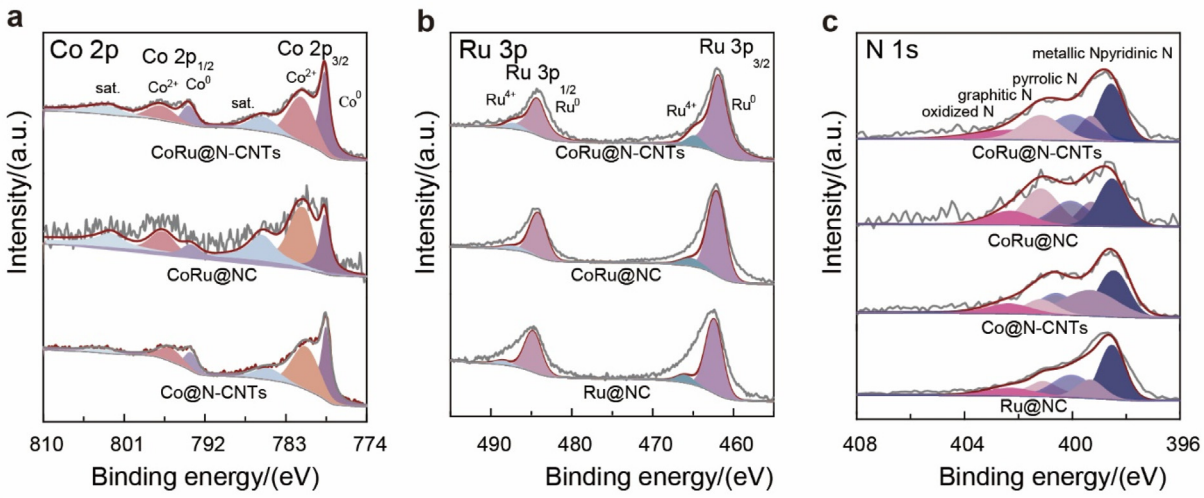

Fig. 3. High-resolution XPS spectra for (a) Co 2p of the CoRu@N-CNTs, CoRu@NC and Co@N-CNTs; (b) Ru 3p of the CoRu@N-CNTs, CoRu@NC and Ru@NC; (c) N 1s of the CoRu@N-CNTs, CoRu@NC, Ru@NC and Co@N-CNTs.

the Co 2p peaks in the CoRu@N-CNTs upshifted to the high binding energy, meanwhile the Ru 3p downshifted compared with those of the Co@N-CNTs and Ru@NC counterparts, indicating a charge transfer occurred between Co and Ru in CoRu@N-CNTs, which was beneficial for the electrochemical reactions. The high-resolution N 1s spectrum of the CoRu@N-CNTs could be deconvoluted into five parts (Fig. 3c), including the pyridinic N (398.56 eV), metallic N (399.3 eV), pyrrolic N (400.00 eV), graphitic N (401.14 eV) and oxidized N (402.5 eV) [38,46]. The presence of M-N (M = Co, Ru) species suggested that N doped in the carbon nanotubes could anchor metal atoms, favoring the formation of diatomic sites. Notably, the pyridinic N can serve as active sites to promote the electrocatalytic HER process [47,48].

3.2. Electrocatalytic performance for CoRu@N-CNTs

To evaluate the electrocatalytic performance of CoRu@N-CNTs, HER measurements were conducted in Ar-saturated 1 mol·L^{-1} KOH with a typical three-electrode system. For comparison, the CoRu@NC, Co@N-CNTs, Ru@NC and commercial Pt/C were selected as references. To be accurate, the reference electrode was calibrated against RHE in H_2-saturated 1 mol·L^{-1} KOH media before all the tests (Fig. S6). Firstly, the HER activity was assessed using linear sweep voltammetry (LSV) with 85% iR-corrections. As shown in Fig. 4a, the CoRu@N-CNTs exhibited an outstanding electrocatalytic activity among all the samples. To achieve a current density of 10 mA·cm^{-2}, the CoRu@N-CNTs merely required an overpotential (η_{10}) of 19 mV, much superior to CoRu@NC (45 mV), Ru@NC (39 mV), Co@N-CNTs (219 mV) and even the commercial benchmark 20% Pt/C (55 mV). The HER kinetics was then assessed by Tafel plots shown in Fig. 4b. Particularly, the CoRu@N-CNTs displayed a Tafel slope of 26.19 mV·dec^{-1}, much smaller than those of the CoRu@NC (65.84 mV·dec^{-1}), Ru@NC (62.41 mV·dec^{-1}), Co@N-CNTs (174.08 mV·dec^{-1}), and the commercial benchmark 20% Pt/C (94.16 mV·dec^{-1}), indicating a favorable electrochemical reaction kinetics of CoRu@N-CNTs [40,46]. The small Tafel slope of CoRu@N-CNTs suggested that the rate-limiting step is the recombination of chemical adsorbed hydrogen and the HER over the catalysts following the Volmer-Tafel mechanism [49,50]. The histograms depicted in Fig. 4c demonstrate the superior catalytic activity of CoRu@N-CNTs and its faster reaction kinetics for the HER. In addition, the charge transfer kinetics of CoRu@N-CNTs, CoRu@NC, Ru@NC, Co@N-CNTs and the commercial benchmark 20% Pt/C were investigated by EIS measurement (Fig. 4d). The charge transfer resistance (R_{ct}) obtained from the semicircle in the low-frequency region of the Nyquist plot is related to the electrocatalytic kinetics at the interface between the electrocatalyst and electrolyte, and a smaller value corresponds to a faster electron transfer. Compared to the CoRu@NC (R_{ct} = 12.51 Ω), Co@N-CNTs (R_{ct} = 28.22 Ω), Ru@NC (R_{ct} = 11.15) and Pt/C (R_{ct} = 25.18), the CoRu@N-CNTs possessed the smallest R_{ct} value of 7.24 Ω, indicative of the fastest reaction rate. To unravel the intrinsic activity of CoRu@N-CNTs, the C_{dl} values were obtained by scanning CV curves in the non-Faradic region (Fig. S7), which is positively proportional to ECSA [21,27]. As shown in Fig. 4e, the CoRu@N-CNTs

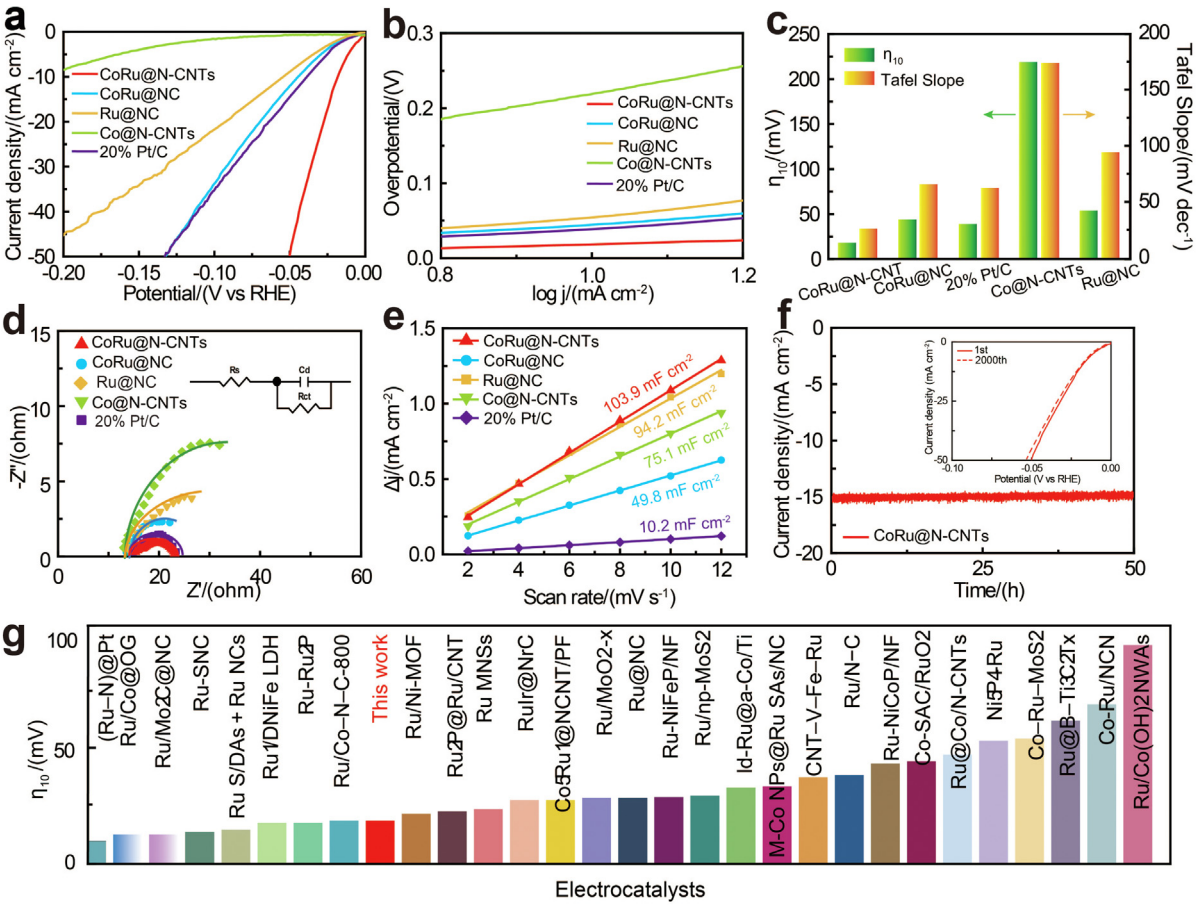

Fig. 4. Electrochemical HER performance in 1.0 mol·L^{-1} KOH. (a) LSV curves, (b) Tafel plots, (c) histograms of overpotential and Tafel slope, (d) Nyquist plots and (e) current density difference plots against scan rate of the CoRu@N-CNTs, CoRu@NC, Ru@NC, Co@N-CNTs and the commercial benchmark 20% Pt/C. (f) Long-term chronoamperometric test of the CoRu@N-CNTs, the inset showing the LSV curves of the CoRu@N-CNTs before (solid) and after (dashed) 2000 CV cycles. (g) Performance comparison of the CoRu@N-CNTs with the recently-reported Co/Ru-based HER electrocatalysts in 1.0 mol·L^{-1} KOH.

delivered a significantly larger C_{dl} value (103.9 mF·cm^{-2}) than those of CoRu@NC (49.8 mF·cm^{-2}), Ru@NC (94.2 mF·cm^{-2}), Co@N-CNTs (75.1 mF·cm^{-2}) and Pt/C (10.2 mF·cm^{-2}). Moreover, the ECSA-normalized LSV further confirmed the excellent intrinsic activity of CoRu@N-CNTs (Fig. S8). To further evaluate the long-term stability of the CoRu@N-CNTs, the chronopotentiograms were also measured as shown in Fig. 4f. It can be seen that the current density remained almost unchanged after 50 h at the current density of 15 mA·cm^{-2}. In addition, the LSV curves after continuously scanning by CV for 2000 cycles displayed negligible decay (the inset of Fig. 4f). Besides, the HER performance of CoRu@N-CNTs surpassed most of the recently reported Co/Ru-based HER electrocatalysts (Fig. 4g and Table S2).

4. Conclusions

In this work, a Co and Ru bimetallic electrocatalyst consisting of CoRu nanoalloy uniformly distributed on N-CNTs (CoRu@N-CNTs) was successfully prepared through hydrothermal reaction of Ru^{3+}, $C_{60}(OH)_n$ and melamine in the presence of Co^{2+}. The as-obtained CoRu@N-CNTs exhibited superior electrocatalytic HER activity in an alkaline condition, *i.e.*, it only needed an overpotential 19 mV to reach a current density of 10 mA·cm^{-2}, with a Tafel slope of 26.19 mV·dec^{-1} in 1 mol·L^{-1} KOH, and good long-term durability. The enhanced electrocatalytic HER performance of CoRu@N-CNTs could be attributed to the following aspects: (1) The electronic communication between Ru and Co sites induced a synergistically electrocatalytic effect, and thus improving the charge distribution of CoRu@N-CNTs, which in turn facilitates the electrocatalytic HER process; (2) The N-CNTs not only served as the electron collector, accelerating the charge transfer between the catalyst and electrolyte, but also provided a tubular channel, which is beneficial to the mass and charge transportations; (3) The synergistic electronic metal-support interaction (EMSI) between the pyridinic N and CoRu bimetallic sites that improved the electronic structure of CoRu@N-CNTs, thus boosting

the electrocatalyst HER performance. This work provides a new idea for the design and construction of novel and efficient electrocatalysts in the field of energy storage and conversion.

Conflict of interest

The authors decline no competing interest.

Acknowledgements

This work was supported by the National Natural Science Foundation of China (No. 52072226, U22A20144), Key Research and Development Program of Shaanxi (2024GX-YBXM-466), Science and Technology Program of Xi'an, China (22GXFW0013), and Science and Technology Program of Weiyang District of Xi'an, China (202315).

References

[1] Qiao M F, Wang Y, Wang Q, Hu G Z, Mamat X, Zhang S S, Wang S Y. Hierarchically ordered porous carbon with atomically dispersed FeN_4 for ultraefficient oxygen reduction reaction in proton-exchange membrane fuel cells[J]. Angew. Chem. Int. Ed., 2020, 59(7): 2688−2694.

[2] Wang J H, Cui W, Liu Q, Xing Z C, Asiri A M, Sun X P. Recent progress in cobalt-based heterogeneous catalysts for electrochemical water splitting[J]. Adv. Mater., 2016, 28(2): 215−230.

[3] Hodges A, Hoang A L, Tsekouras G, Wagner K, Lee C Y, Swiegers G F, Wallace G G. A high-performance capillary-fed electrolysis cell promises more cost-competitive renewable hydrogen[J]. Nat. Commun., 2022, 13(1): 1304.

[4] Chu C H, Huang D H, Gupta S, Weon S, Niu J F, Stavitski E, Muhich C, Kim J H. Neighboring Pd single atoms surpass isolated single atoms for selective hydrodehalogenation catalysis[J]. Nat. Commun., 2021, 12(1): 5179.

[5] Kang J X, Qiu X Y, Hu Q, Zhong J, Gao X, Huang R, Wan C Z, Liu L M, Duan X F, Guo L. Valence oscillation and dynamic active sites in monolayer NiCo hydroxides for water oxidation[J]. Nat. Catal., 2021, 4(12): 1050−1058.

[6] Gao T T, Li X Q, Chen X J, Zhou C X, Yue Q, Yuan H Y, Xiao D. Ultra-fast preparing carbon nanotube-supported trimetallic Ni, Ru, Fe heterostructures as robust bifunctional electrocatalysts for overall water splitting[J]. Chem. Eng. J., 2021, 424: 130416.

[7] Wang T J, Jiang Y C, He J W, Li F M, Ding Y, Chen P, Chen Y. Porous palladium phosphide nanotubes for formic acid electrooxidation[J]. Carbon Energy, 2022, 4(3): 283−293.

[8] Jiang W J, Tang T, Zhang Y, Hu J S. Synergistic modulation of non-precious-metal electrocatalysts for advanced water splitting[J]. Acc. Chem. Res., 2020, 53(6): 1111−1123.

[9] Huang C, Ouyang T, Zou Y, Li N, Liu Z Q. Ultrathin $NiCo_2Px$ nanosheets strongly coupled with CNTs as efficient and robust electrocatalysts for overall water splitting [J]. J. Mater. Chem. A, 2018, 6(17): 7420−7427.

[10] Olabi A G, Abdelkareem M A. Renewable energy and climate change[J]. Renew. Sustain. Energy Rev., 2022, 158: 112111.

[11] Wang X N, Zhao L M, Li X J, Liu Y, Wang Y S, Yao Q F, Xie J P, Xue Q Z, Yan Z F, Yuan X, Xing W. Atomic-precision Pt_6 nanoclusters for enhanced hydrogen electro-oxidation [J]. Nat. Commun., 2022, 13(1): 1596.

[12] Zaman S, Huang L, Douka A I, Yang H, You B, Xia B Y. Oxygen reduction electrocatalysts toward practical fuel cells: progress and perspectives[J]. Angew. Chem. Int. Ed., 2021, 60(33): 17832−17852.

[13] Chen H, Zhang B, Liang X, Zou X X. Light alloying element-regulated noble metal catalysts for energy-related applications[J]. Chin. J. Catal., 2022, 43(3): 611−635.

[14] Sun Y M, Xue Z Q, Liu Q L, Jia Y L, Li Y L, Liu K, Lin Y Y, Liu M, Li G Q, Su C Y. Modulating electronic structure of metal-organic frameworks by introducing atomically dispersed Ru for efficient hydrogen evolution[J]. Nat. Commun., 2021, 12(1): 1369.

[15] Clay C, Haq S, Hodgson A. Intact and dissociative adsorption of water on Ru(0001)[J]. Chem. Phys. Lett., 2004, 388(1): 89−93.

[16] Cao X J, Huo J J, Li L, Qu J P, Zhao Y F, Chen W H, Liu C T, Liu H, Wang G X. Recent advances in engineered Ru-based electrocatalysts for the hydrogen/oxygen conversion reactions[J]. Adv. Energy Mater., 2022, 12(41): 2202119.

[17] Liu Z, Zeng L L, Yu J Y, Yang L J, Zhang J, Zhang X L, Han F, Zhao L L, Li X, Liu H, Zhou W J. Charge redistribution of Ru nanoclusters on Co_3O_4 porous nanowire via the oxygen regulation for enhanced hydrogen evolution reaction[J]. Nano. Energy, 2021, 85: 105940.

[18] Wang Y J, Luo W J, Li H J, Cheng C AW. Ultrafine Ru nanoclusters supported on N/S doped macroporous carbon spheres for efficient hydrogen evolution reaction[J]. Nanoscale Adv., 2021, 3(17): 5068−5074.

[19] Wu Y L, Li X, Wei Y S, Fu Z, Wei W, Wu X T, Zhu Q L, Xu Q. Ordered macroporous superstructure of nitrogen-doped nanoporous carbon implanted with ultrafine Ru nanoclusters for efficient pH-universal hydrogen evolution reaction[J]. Adv. Mater., 2021, 33(12): 2006965.

[20] Zhang X L, Ma J, Yan R W, Cheng W X, Zheng J, Jin B K. Pt-Ru/polyaniline/carbon nanotube composites with three-layer tubular structure for efficient methanol oxidation[J]. J. Alloys Compd., 2021, 867: 159017.

[21] Zhai P L, Xia M Y, Wu Y Z, Zhang G H, Gao J F, Zhang B, Cao S Y, Zhang Y T, Li Z W, Fan Z Z, Wang C, Zhang X M, Miller J T, Sun L C, Hou J G. Engineering single-atomic ruthenium catalytic sites on defective nickel-iron layered double hydroxide for overall water splitting[J]. Nat. Commun., 2021, 12(1): 4587.

[22] Han X, Li Y J, Wang X, Dong J T, Li H M, Yin S, Xia J X. Ru anchored on $Co(OH)_2$ nanowire arrays as highly effective electrocatalyst for full water splitting[J]. Int. J. Hydrogen Energy, 2024, 51: 769−776.

[23] Liu Z, Yang X D, Hu G Z, Feng L G. Ru nanoclusters coupled on Co/N-doped carbon nanotubes efficiently catalyzed the hydrogen evolution reaction[J]. ACS Sustainable Chem. Eng., 2020, 8(24): 9136−9144.

[24] Shah K, Dai R Y, Mateen M, Hassan Z, Zhuang Z W, Liu C H, Israr M, Cheong W C, Hu B T, Tu R Y, Zhang C, Chen X, Peng Q, Chen C, Li Y D. Cobalt single atom incorporated in ruthenium oxide sphere: a robust bifunctional electrocatalyst for HER and OER[J]. Angew. Chem. Int. Ed., 2022, 61(4): e202114951.

[25] Martínez-Séptimo A, Valenzuela M A, Del Angel P, González-Huerta G R. Irruox/TiO_2 a stable electrocatalyst for the oxygen evolution reaction in acidic media[J]. Int. J. Hydrogen Energy, 2021, 46(51): 25918−25928.

[26] Li G K, Jang H, Liu S G, Li Z J, Kim M G, Qin Q, Liu X, Cho J. The synergistic Effect of Hf-O-Ru Bonds and oxygen vacancies in Ru/HfO_2 for enhanced hydrogen evolution[J]. Nat. Commun., 2022, 13(1): 1270.

[27] Feng W H, Feng Y Q, Chen J S, Wang H, Hu Y Z, Luo T M, Yuan C K, Cao L Y, Feng L L, Huang J F. Interfacial electronic engineering of Ru/FeRu nanoparticles as efficient trifunctional electrocatalyst for overall water splitting and Zn-Air battery[J]. Chem. Eng. J., 2022, 437: 135456.

[28] Lin S Y, Chen Y P, Cao Y, Zhang L, Feng J J, Wang A J. Aminouracil-assisted synthesis of CoFe decorated bougainvillea-like N-doped carbon nanoflowers for boosting Zn-Air battery and water electrolysis[J]. J. Power Sources, 2022, 521: 230926.

[29] Song H Q, Wu M, Tang Z Y, Tse J S, Yang B, Lu S Y. Single atom ruthenium-doped CoP/CDs nanosheets via splicing of carbon-dots for robust hydrogen production[J]. Angew. Chem. Int. Ed., 2021, 60(13): 7234−7244.

[30] Kumar A, Bui V Q, Lee J, Wang L, Jadhav A R, Liu X, Shao X, Liu Y, Yu J, Hwang Y, Bui H TD, Ajmal S, Kim M G, Kim S G, Park G S, Kawazoe Y, Lee H. Moving beyond bimetallic-alloy to single-atom dimer atomic-interface for all-pH hydrogen evolution[J]. Nat. Commun., 2021, 12(1): 6766.

[31] Lu Z Y, Wang B F, Hu Y F, Liu W, Zhao Y F, Yang R O, Li Z P, Luo J, Chi B, Jiang Z, Li M S, Mu S C, Liao S J, Zhang J J, Sun X L. An isolated zinc-cobalt atomic pair for highly active and durable oxygen reduction[J]. Angew. Chem. Int. Ed., 2019, 58(9): 2622−2626.

[32] Bai L, Hsu C S, Alexander D TL, Chen H M, Hu X. Double-atom catalysts as a molecular platform for heterogeneous oxygen evolution electrocatalysis[J]. Nat. Energy, 2021, 6(11): 1054−1066.

[33] Liu D B, Zhao Y, Wu C Q, Xu W J, Xi S B, Chen M X, Yang L, Zhou Y Z, He Q, Li X Y, Ge B H, Song L, Jiang J, Yan Q Y. Triggering electronic coupling between neighboring hetero-diatomic metal sites promotes hydrogen evolution reaction kinetics[J]. Nano. Energy, 2022, 98: 107296.

[34] Li J Z, Hou C Z, Chen C, Ma W S, Li Q, Hu L W, Lv X W, Dang J. Collaborative interface optimization strategy guided ultrafine RuCo and Mxene heterostructure electrocatalysts for efficient overall water splitting[J]. ACS Nano., 2023, 17(11): 10947−10957.

[35] Su K Y, Yang S, Yang A Z, Guo Y, Liu B, Zhu J W, Tang Y W, Qiu X Y. Customizing the anisotropic electronic states of Janus-distributive FeN_4 and NiN_4 dual-atom sites for reversible oxygen electrocatalysis[J]. Appl. Catal. B Environ., 2023, 331: 122694.

[36] Luo T M, Huang J F, Hu Y Z, Yuan C K, Chen J S, Cao L Y, Kajiyoshi K, Liu Y J, Zhao Y, Li Z J, Feng Y Q. Fullerene lattice-confined Ru nanoparticles and single atoms synergistically boost electrocatalytic hydrogen evolution reaction [J]. Adv. Funct. Mater., 2023, 33(12): 2213058.

[37] Wei C, Rao R R, Peng J, Huang B, Stephens I EL, Risch M, Xu Z J, Shao-Horn Y. Recommended practices and benchmark activity for hydrogen and oxygen electrocatalysis in water splitting and fuel cells[J]. Adv. Mater., 2019, 31(31): 1806296.

[38] Chen J, Huang J, Wang R, Feng W, Wang H, Luo T, Hu Y, Yuan C, Feng L, Cao L, Kajiyoshi K, He C, Liu Y, Li Z, Feng Y. Atomic ruthenium coordinated with chlorine and nitrogen as efficient and multifunctional electrocatalyst for overall water splitting and rechargeable zinc-air battery[J]. Chem. Eng. J., 2022, 441: 136078.

[39] Feng Y Q, Li X, Liu Q Q, Zhu W J, Huo X M, Gao M T, Liu W W, Wang Y, Wei Y. Fullerene-derived nanocomposite as an efficient electrocatalyst for overall water splitting and Zn-air battery[J]. Mater. Chem. Front., 2023, 7(24): 6446−6462.

[40] Chen J S, Huang J F, Zhao Y, Cao L Y, Kajiyoshi K, Liu Y J, Li Z J, Feng Y Q. Enhancing the electronic metal-support interaction of CoRu alloy and pyridinic N for electrocatalytic pH-universal hydrogen evolution reaction[J]. Chem. Eng. J., 2022, 450: 138026.

[41] Duan S S, Han G S, Su Y H, Zhang X Y, Liu Y Y, Wu X L, Li B J. Magnetic Co@G-C_3N_4 core-shells on rGO sheets for momentum transfer with catalytic activity toward continuous-flow hydrogen generation[J]. Langmuir, 2016, 32(25): 6272−6281.

[42] Zhang F F, Zhu Y L, Chen Y, Lu Y ZH, Lin Q, Zhang L, Tao S W, Zhang X W, Wang H T. RuCo alloy bimodal nanoparticles embedded in N-doped carbon: a superior pH-universal electrocatalyst outperforms benchmark Pt for the hydrogen evolution reaction[J]. J. Mater. Chem. A, 2020, 8(25): 12810−12820.

[43] Zhang M L, Wang J L, Zhang Y Q, Ye L, Gong Y Q. Ultrafine CoRu alloy nanoparticles *in situ* embedded in Co_4N Porous nanosheets as high-efficient hydrogen evolution electrocatalysts[J]. Dalton Trans, 2021, 50(8): 2973−2980.

[44] Chen J, Ha Y, Wang R R, Liu Y X, Xu H B, Shang B, Wu R B, Pan H G. Inner Co synergizing outer Ru supported on carbon nanotubes for efficient pH-universal hydrogen evolution catalysis[J]. Nano-Micro Lett., 2022, 14(1): 186.

[45] Cao D, Wang J Y, Xu H X, Cheng D J. Construction of dual-site atomically dispersed electrocatalysts with Ru-C_5 single atoms and Ru-O_4 nanoclusters for accelerated alkali hydrogen evolution[J]. Small, 2021, 17(31): 2101163.

[46] Tiwari J N, Harzandi A M, Ha M, Sultan S, Myung C W, Park H J, Kim D Y, Thangavel P, Singh A N, Sharma P, Chandrasekaran S S, Salehnia F, Jang J W, Shin H S, Lee Z, Kim K S. High-performance hydrogen evolution by Ru single atoms and nitrided-Ru nanoparticles implanted on N-Doped graphitic sheet[J]. Adv. Energy Mater., 2019, 9(26): 1900931.

[47] Zhao D, Sun K A, Cheong W C, Zheng L R, Zhang C, Liu S J, Cao X, Wu K L, Pan Y, Zhuang Z W, Hu B T, Wang D S, Peng Q, Chen C, Li Y D. Synergistically interactive pyridinic-N-MoP sites: identified active centers for enhanced hydrogen evolution in alkaline solution[J]. Angew. Chem. Int. Ed., 2020, 59(23): 8982−8990.

[48] Yu W H, Huang H, Qin Y N, Zhang D, Zhang Y Y, Liu K, Zhang Y, Lai J P, Wang L. The synergistic effect of pyrrolic-N and pyridinic-N with Pt under strong metal-support interaction to achieve high-performance alkaline hydrogen evolution[J]. Adv. Energy Mater., 2022, 12(21): 2200110.

[49] Chen Y W, Ding R, Li J, Liu J G. Highly active atomically dispersed platinum-based electrocatalyst for hydrogen evolution reaction achieved by defect anchoring strategy[J]. Appl. Catal. B Environ., 2022, 301: 120830.

[50] Su P P, Pei W, Wang X W, Ma Y F, Jiang Q K, Liang J, Zhou S, Zhao J J, Liu J, Lu G Q. Exceptional electrochemical HER performance with enhanced electron transfer between Ru nanoparticles and single atoms dispersed on a carbon substrate[J]. Angew Chem. Int. Ed., 2021, 60(29): 16044−16050.

氮掺杂碳纳米管上钴和钌位点之间的电子通信促进碱性析氢反应

高梦婷#，卫　莹#，霍雪萌，朱文洁，刘箐箐，强晋源，刘婉婉，王　颖，李　旭，黄剑锋，冯永强*
陕西科技大学材料科学与工程学院，西安 710021

摘要

碱性电解水析氢反应作为获取绿色氢能源的重要途径具有广泛的研究意义和应用价值，但其缓慢的电极反应动力学及较高的过电位需要高效稳定的催化剂来加速反应过程。目前商用的铂（Pt）基催化剂因高昂的成本限制了其规模化应用。设计高效、低过电位的非 Pt 电催化剂仍然是一个重大挑战。钌（Ru）基催化剂因具有类 Pt 的活性氢结合能而受到广泛关注。本文以富勒醇和三聚氰胺为基体原料，与氯化钴和氯化钌在 150 °C 水热反应 24 小时，随后在氩气/氢气（5%）混合气氛下 600 °C 热解处理，成功在氮掺杂碳纳米管（N-CNTs）上修饰了钴钌（CoRu）纳米合金，制备了一种新型高效的 Co，Ru 双金属电催化剂。得益于 Co 和 Ru 位点之间的电子通信，所得 CoRu@N-CNTs 具有优异的电催化析氢反应活性。在 1 mol·L^{-1} 氢氧化钾水溶液中达到 10 mA·cm^{-2} 的电流密度，所需过电位仅为 19 mV，塔菲尔斜率为 26.19 mV·dec^{-1}，优于基准 Pt/C 催化剂。本研究将为高效析氢电催化剂的设计与制造开辟一条新的道路，有力推动电解水制氢技术在能源存储与转化领域的应用推广，为我国“碳达峰与碳中和”战略目标的实施蓄势赋能。

关键字：钴钌合金；电催化剂；水裂解；析氢反应；碳纳米管